Corrosion Mechanism in Artificial Sweat Solution of In-Bearing White Bronze Alloy

Corrosion Mechanism in Artificial Sweat Solution of In-Bearing White Bronze Alloy

S. Caporali[‡,] and U. Bardi[*]*

ABSTRACT

Corrosion properties of thin layers of a copper-tin-zinc-indium alloy ("white bronze") were investigated in an artificial sweat solution indicating poor resistance properties. The coating degraded via pitting, generalized, and crevice corrosion, as evidenced by scanning electron microscopy-energy-dispersive x-ray analysis (SEM-EDX) investigation. The corrosion mechanism was investigated in situ by means of electrochemical impedance spectroscopy (EIS), and ex situ by x-ray photoelectron spectroscopy (XPS). These combined results demonstrate that the key point of the corrosion failure is the removal of the passive In-Sn oxides.

KEY WORDS: artificial sweat, coating, copper, crevice corrosion, electrochemical impedance spectroscopy, generalized corrosion, indium, pitting, tin, white bronze, x-ray photoelectron spectroscopy, zinc

INTRODUCTION

Presently, nickel electroplating is one of the most diffuse finishing technologies for decorative coatings, especially in the jewelry industry. The reasons of the success of this method are a result of the nickel physico-chemical characteristics, as well as the ease of nickel electrodeposition. By tuning the electrodeposition parameters, it is possible to deposit nickel coatings, which are very homogeneous and hard, with excellent anticorrosion properties, and bright with a fashionable silvery-white finish. Therefore, this technique is used now widely for surface-finishing of commonly used objects such as belt buckles, clasps, wrist watches, keys, spectacle frames, zippers, clips, buttons, earrings, etc.

However, the wide use of this metal in everyday life has also resulted in problems. Once rare, allergic contact dermatitis is now recognized as a significant health issue, and nickel has received much attention for being one of the most common sensitizing agent for this pathology. Galvanization eczema (nickel contact allergy), historically referred to as hand dermatitis in miners, is now diffused especially among women and teens, probably because of increased skin contact with nickel-releasing jewelry.[1-4]

In Europe, 10% to 15% of adult females and 1% to 3% of adult males are allergic to nickel,[5-7] and even larger fractions of the population are affected in the United States.[8-10]

The alarming frequency of sensitization to nickel led to this metal being named the 2008 "Allergen of the Year" by the American Contact Dermatitis Society.[11] Consequently, the European Union (EU) issued the directive 94/27/EC, named "The Nickel Directive," limiting the rate of nickel release to 0.5 μg cm^{-2} $week^{-1}$ for objects that come into direct and prolonged contact with the skin.[12] Recently, two more directives were issued to reduce further the nickel permitted release down to 0.2 μg cm^{-2} $week^{-1}$ from "post assemblies"[12] and extend these limits to nickel compounds.[13]

Since the end of the 1990s, several studies were carried out to determine, and eventually reduce, Ni

Submitted for publication June 29, 2011; in revised form, August 17, 2011.

‡ Corresponding author. E-mail: stefano.caporali@unifi.it.

* Chemistry Department, Università di Firenze, Via della Lastruccia, 3 – 50019 Sesto Fiorentino (FI), Italy, and Consorzio Interuniversitario Nazionale di Scienza e Tecnologia dei Materiali (INSTM), Via Giusti, 9 – 50147 Firenze (FI), Italy.

ISSN 0012-9312 (print), 1938-159X (online)
12/000021/$5.00+$0.50/0

release from objects designed to be in contact with the human body, such as medical devices,[14-19] cutlery,[20-21] coins,[22-23] and guitar strings,[24] in various types of synthetic body fluids.[25-30]

However, all these studies have focused on the properties of bulk materials, leaving the field of decorative coatings practically unexplored. Apart from the enormous industrial interest, very few studies have been carried out so far with the goal of achieving an economically affordable and viable alternative to the conventional nickel-electroplating process.[31-32] Aluminium was proposed,[33] because of its outstanding corrosion resistance, but the aesthetic results were not satisfying for fashion accessories.

Gold- and palladium-based alternatives do exist, but their relatively high cost make their use not suitable for top-finishing of large-scale production goods.

Copper-based alloys, such as copper-tin ("yellow bronzes") and copper-tin-zinc ("white bronzes"), were also proposed as topcoats or undercoats. These alloys are characterized by good anticorrosion properties, especially in aggressive industrial environments such as sulfur dioxide (SO_2)-containing atmosphere (Kesternich Test, DIN 50018).[34] However, even if bright yellow bronzes can be electrodeposited easily,[35] their color restricts the field of applications for aesthetic purposes. On the other hand, white bronze alloy coatings tend to be porous,[36] which causes them to be more prone to preferential localized attack at the pore site in corrosive and chloride-bearing environments such as sweat and other body fluids. Recently, to overcome this issue, the addition of indium up to 10 wt% to the "white bronze" composition was proposed. A plating bath and a method for the electrodeposition of the quaternary copper-tin-zinc-indium alloy were patent protected by Enthone, Inc. (West Haven, Connecticut).[37] The mechanical and aesthetic properties of the electroplated indium-bearing white bronze coatings are very similar to those of the electroplated nickel; but, with nickel being virtually absent in this alloy, its use does not threaten the customer's heath. Preliminary studies[38] evidenced outstanding anticorrosion properties in a neutral saline environment but scarce resistance in pickling solution environment, making its use not suitable for goods designed to be in contact with skin.

In this paper, the corrosion behavior of copper-tin-zinc-indium-coated brass samples were evaluated in an artificial sweat solution using electrochemical (potentiodynamic, open-circuit potential [OCP]), and electrochemical impedance spectroscopy [EIS]) and free corrosion tests. In situ (electrochemical) and ex situ (x-ray photoelectron spectroscopy [XPS] and scanning electron microscopy-energy-dispersive x-ray analysis [SEM-EDX]) investigations were carried out to determine the corrosion mechanism.

EXPERIMENTAL PROCEDURES

UNS C46400[(1)] (Naval brass 464 lead-free [wt% 59 to 62 copper, 36.7 to 40.2 zinc, 0.2 lead, 0.1 iron, 0.5 to 1 tin, density: 8.41 $g \cdot cm^{-3}$]), in the form of 5 cm by 5 cm laminae, was used as the substrate. The reference samples were produced depositing 20 μm to 25 μm of nickel from a commercial Watt-type electroplating bath. Indium-bearing white bronze ("Indium-WB" throughout the text) layers (composition wt%: 50 to 54 Cu, 7 to 9 Zn, 25 to 35 Sn, and 9 to 11 In) 1 μm thick were electrodeposited as described in the literature[37] on copper-coated brass (15 μm of copper electrodeposited from a commercial acid bath made with 150 g/L copper sulfate [Cu_2SO_4], 25 g/L sulfuric acid [H_2SO_4], 10 g/L ammonium sulfate [$(NH_4)_2SO_4$], T = 25±5°C). The composition of the Indium-WB alloy, as well as the chemical homogeneity, was verified using EDX analysis sampling at least 7 points on every sample. All the measurements gave elemental values in accordance with the Indium-WB nominal composition and no significative differences were observed within the samples.

Both electrochemical and free corrosion tests were carried out in the same artificial sweat solution prepared by dissolving 20 g/L sodium chloride (NaCl), 17.5 g/L ammonium chloride (NH_4Cl), 5 g/L urea (CH_4N_2O), 2.5 ml/L acetic acid ($C_2H_4O_2$), 15 ml/L lactic acid ($C_3H_6O_3$) (all pure reagent) in deionized water and adjusting the pH up to 4.7 with sodium hydroxide (NaOH) solution.

Free corrosion tests were performed in accordance with the standard used in jewelry and in the fashion industry (ISO 3160-2).[39] Three samples for each type of coating were placed on a cotton pad soaked with artificial sweat and kept into a thermostatically controlled (40±3°C) sealed box. After 24 h, the part of the samples that stayed in contact with the pad was rinsed carefully with deionized water and acetone (CH_3COCH_3), air-dried, and examined.

SEM was performed with a microscope equipped with EDX microanalysis. Semiquantitative analysis of the sample composition surfaces were achieved by fitting the EDX peaks by Gaussian-type curves and applying the Proza (Phi-Rho-Z) correction method.

XPS measurements were performed in an ultra-high vacuum (10^{-9} mbar) system equipped with a VSW HAC 5000[†] hemispherical electron energy analyzer and a non-monochromatized Al-Kα x-ray source (1,486.6 eV). The source power was 100 W (10 kV × 10 mA) and the spectra were acquired in the constant-pass-energy mode at E_{pas} = 44 eV. The overall energy resolution was 1.2 eV as a full-width at half maximum (FWHM) for the Ag $3d_{5/2}$ line of a pure silver reference. No neutralizer was utilized and the spectra

[(1)] UNS numbers are listed in *Metals and Alloys in the Unified Numbering System*, published by the Society of Automotive Engineers (SAE International) and cosponsored by ASTM International.

[†] Trade name.

energy scale was corrected using the carbon 1s peak (284.8 eV) of adventitious atmospheric contamination. After subtraction of a Shirley-type background, the recorded spectra were fitted using software with Gauss-Lorentz curves. Semiquantitative elemental analysis was carried out using sensitivity factors available in the literature.[40]

Electrochemical characterization was performed using a corrosion cell from Princeton Applied Research (flat cell KO235†) and a PAR model 2273† potentiostat controlled by PowerSuite 2.58† software. A classical three-electrode setup was using with platinum mesh as the counter electrodes and a saturated calomel electrode (SCE) reference electrode separated from the solution with an ion-conducting glass frit. The potential of the reference electrode was controlled monthly, and if it was found to exceed the expected value (0.241 V vs. standard hydrogen electrode [SHE]) for more than 0.002 V, the potassium chloride (KCl) solution and glass frit were replaced. The exposed working electrode surface was 1.0 cm^2 in all the electrochemical experiments. Every sample was kept in the test solution for at least 18 h to allow the stabilization of the system. During this time, the OCP was recorded. Then, EIS and potentiodynamic (PD) tests were performed. The EIS spectra were measured in the frequency range between 100 kHz and 5 mHz, sampling 20 frequencies per decade at different potentials applying a sinusoidal perturbation of ±10 mV. The PD curves were recorded starting from –0.250 V with respect to the free corrosion potential at the scan rate of 0.3 mV s^{-1}. The reproducibility of the electrochemical data was checked by triplicate measurements and typical results are reported here.

RESULTS AND DISCUSSION

Electrochemical Corrosion Tests on Indium-WB-Coated Samples

OCP curves were recorded in aerated artificial sweat solution as a function of time. The results obtained on Indium-WB-coated and reference nickel-coated samples are shown in Figure 1.

Both curves indicate high reactivity in this environment. The reference Ni sample OCP starts from noble values (–0.05 V_{SCE}) and undergoes a progressive reduction down to values close to the Indium-WB-coated ones. This behavior indicates a progressive degradation of the surface layer that becomes gradually more prone to corrosion. On the contrary, the Indium-WB-coated samples always present more active potentials (about –0.27 V_{SCE}), consistent with the "less noble" character of this alloy.

PD curves (Figure 2) were recorded to shed some light on the corrosion processes taking place at the surface. Even though all the samples display similar free corrosion potentials, the anodic branch of these curves presents significant differences between traditional nickel-coated and Indium-WB-coated samples. Nickel coatings show a large potential interval (up to 0.25 V_{SCE}) where the current slightly increases (j_{trans}) (transpassive behavior) before starting a steep increase of almost three orders of magnitude in intensity at about 0.3 V_{SCE}. This phenomenon is well known and has been associated with the breaking down of the passive nickel-oxides layer and the starting of pitting corrosion.[41-43] On the contrary, the anodic current recorded on Indium-WB-coated samples shows three distinct regions:

—a Tafel region at lower overpotentials extending to the peak current density (j_{peak}) (zone 1 in Figure 2)

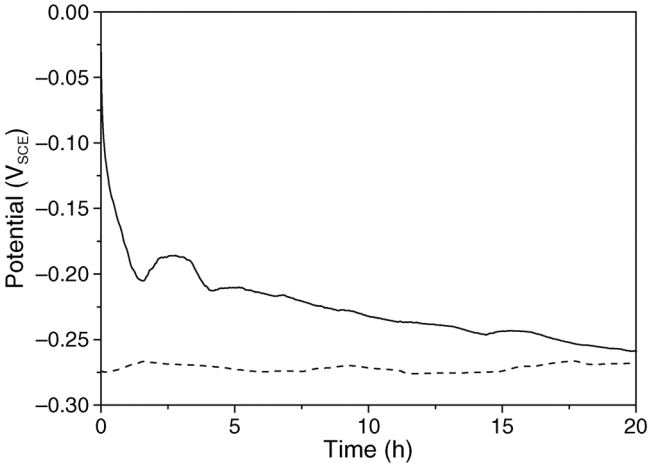

FIGURE 1. *OCP of Indium-WB-coated (dash curve) compared with the reference nickel (solid curve) in artificial sweat solution as a function of time.*

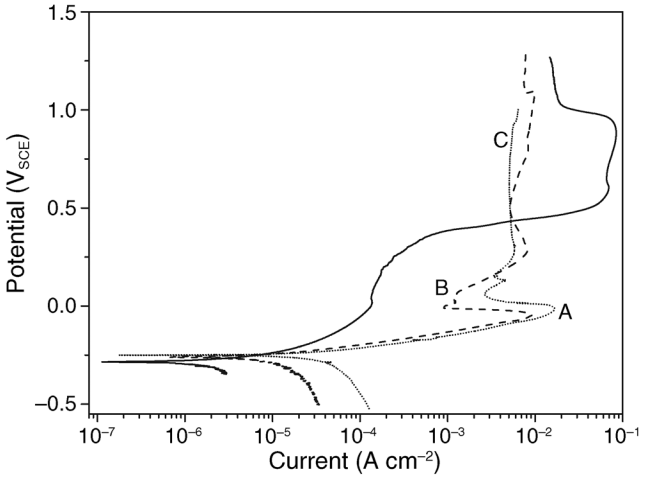

FIGURE 2. *Potentiodynamic curves (scan rate: 0.3 mV/s) of Indium-WB-coated (dash curve) compared with reference nickel one (solid curve) and pure copper (dot curve) in artificial sweat solution. The numbers indicate the three distinct regions of potential on which the reaction that takes place at the electrode differs as described in the text.*

TABLE 1

Electrochemical Corrosion Data of the Indium-WB-Coated Samples Compared with the Traditional Nickel-Coated Ones and Pure Copper, in Artificial Sweat Environment

Sample	j_{trans} (A·cm^{-2})	j_{peak} (A·cm^{-2})	j_{min} (A·cm^{-2})	j_{lim} (A·cm^{-2})
Reference nickel	$2\pm0.5\times10^{-4}$	—	—	$2\pm1\times10^{-2}$
Pure copper	—	$2\pm0.3\times10^{-2}$	$3\pm0.3\times10^{-2}$	$5\pm1\times10^{-3}$
Indium-WB-coated	—	$1\pm0.3\times10^{-2}$	$1\pm0.3\times10^{-3}$	$7\pm2\times10^{-3}$

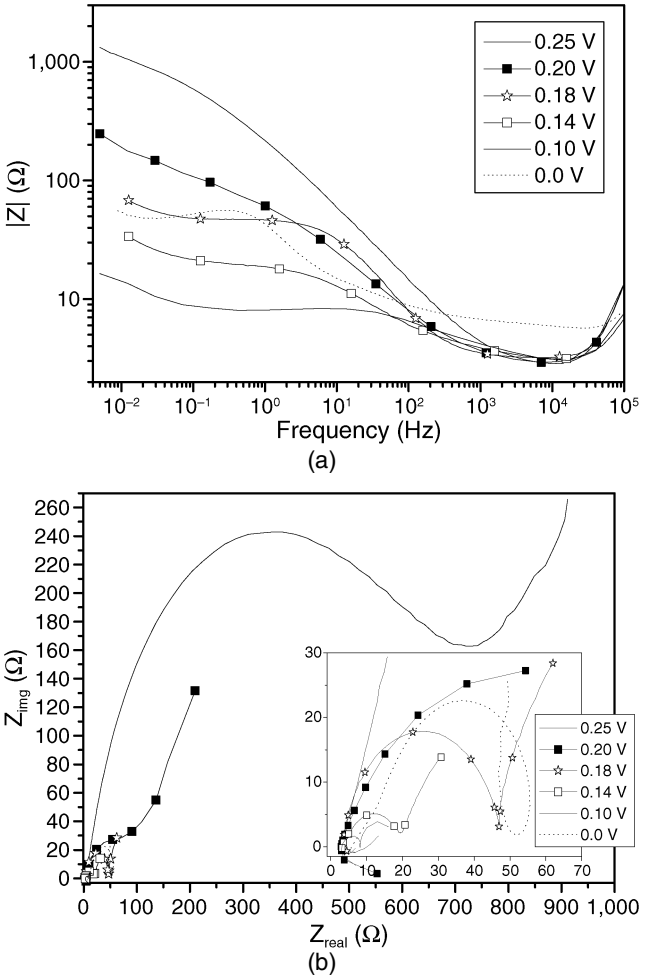

FIGURE 3. *EIS spectra ([A] Bode plots, [B] Nyquist plot) obtained on Indium-WB-coated samples in artificial sweat solution at different potentials. Inset of Figure 3(b) displays a detail of the region. Potentials as described in the legend.*

—a tiny region of decreasing currents until a minimum (j_{min}) (passive behavior) (zone 2 in Figure 2)

—a region of increasing currents leading to a limiting value (j_{lim}) (zone 3 in Figure 2)

This curve closely resembles the curve obtained on pure copper (dot curve in Figure 2). The corrosion mechanism for pure copper in aerated, chloride-bearing pickling solutions is a well-known process. It involves the metal dissolution through oxidation of copper(0) to copper(I), then the copper(I) to copper(II).[44-45] The three regions are interpreted as follow:

—oxidation of metallic copper and formation of copper ions (zone 1)

—formation of labile insoluble copper(I) chloride, which provides only a modest corrosion protection (zone 2)[46-47]

—dissolution of the copper(I) chloride layer by the formation of soluble cuprous chloride complex (zone 3)[48]

In the light of the good analogy between the shape of these two curves, it can be assumed that in this environment, the copper-based alloy Indium-WB's corrosion mechanism is dominated by copper, relegating the other elements to a marginal role in the process.

However, corrosion currents recorded on the Indium-WB sample are somewhat lower than for pure copper (Table 1). Therefore, the presence of other elements, especially tin and indium, appears to contribute to mitigating the severity of the corrosion process. Nevertheless, unlike the case of neutral saline solutions[38] where the corrosion currents of Indium-WB-coated samples are similar to the reference nickel-coated sample, with artificial sweat they are at least one order of magnitude higher (Table 1).

To have a direct insight of the surface evolution during the potential scan, we performed EIS measurement experiments varying the potential between –0.25 V_{SCE} and 0.00 V_{SCE}. In Figure 3(a), we show these data in the form of Bode plots. The most evident effect is that the absolute impedance decreases with potential values moving from active to noble. This occurs in particular in the lowest frequency range, reaching a minimum for the experiments performed at –0.10 V_{SCE} (solid curve in Figure 3[a]). A further shift of the potential toward more noble values (0.00 V_{SCE}) results in an increase of the absolute impedance over the whole frequency range (dot curve in Figure 3[a]). This observation is consistent with the formation of a surface by-product layer capable of slightly decreasing the corrosion rate. Plotting the impedance data in the form of Nyquist diagrams (Figure 3[b]) helps to visualize that over the frequency range examined, the experimental data show an arc-like behavior. This result suggests that corrosion of the samples has occurred in these conditions. It is also evident that the diameter of the semicircle is inversely related to the value of the applied potential (inset, Figure 3[b]). This result implies that the polarization resistance (R_p) also decreases, which, in turn, increases the corrosion rate of the sample.[49] Again, the experiment performed at

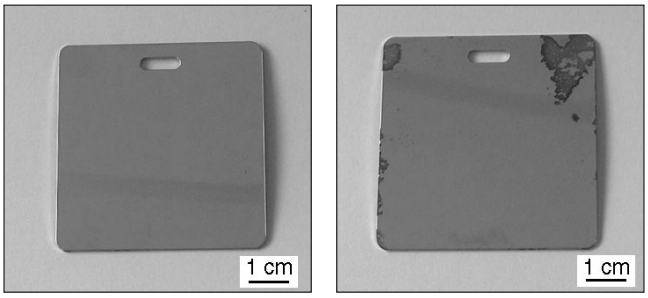

FIGURE 4. *Photos of the samples after free corrosion test in artificial sweat: (a) reference nickel and (b) Indium-WB-coated.*

0.0 V_{SCE} shows an increase of the semicircle diameter consistent with the formation of a new protective layer and the reduction of the corrosion rate.

Free Corrosion Test and Scanning Electron Microscopy Investigation

Figure 4 shows photos of the reference nickel (Figure 4[a]) and Indium-WB-coated (Figure 4[b]) samples after the free corrosion test in artificial sweat solution. In accordance with the electrochemical test, the Indium-WB-coated one is heavily damaged (brown haloes).

The morphological investigation of the damaged parts, carried out by SEM, indicated the presence of narrow pits, crevice, and general corrosion features (Figure 5).

Elemental EDX mapping was used to show surface compositional modifications and the selective depletion of tin from the damaged areas up to the complete removal of the coating (the signal attributable to tin disappears), exposing the copper layer beneath (Figure 6) and the formation of corrosion by-product (chlorides).

X-Ray Photoelectron Spectroscopy Investigation

Because of its extreme surface sensitivity (probing depth: 3 nm to 5 nm)[50] and the possibility to detect different oxidation states of the same element, XPS is especially suitable for monitoring surfaces' evolution. Therefore, Indium-WB-coated samples were examined using XPS before and after the free corrosion tests.

The XPS survey spectra (not displayed here) showed peaks attributable to carbon, oxygen, copper, indium, zinc, tin (all the samples), and chlorine (only after corrosion tests). However, the relative peak intensities changed dramatically before and after exposure to the pickling solution (Figure 7). An accurate quantitative evaluation of the atomic surface composition by XPS is difficult because of the uncertainties in the elemental sensitivity factors (S_f) and on instrumental and matrix effects. However, a semi-quantitative evaluation is possible using tabulated sensitivity factors.[40] Such an analysis is useful

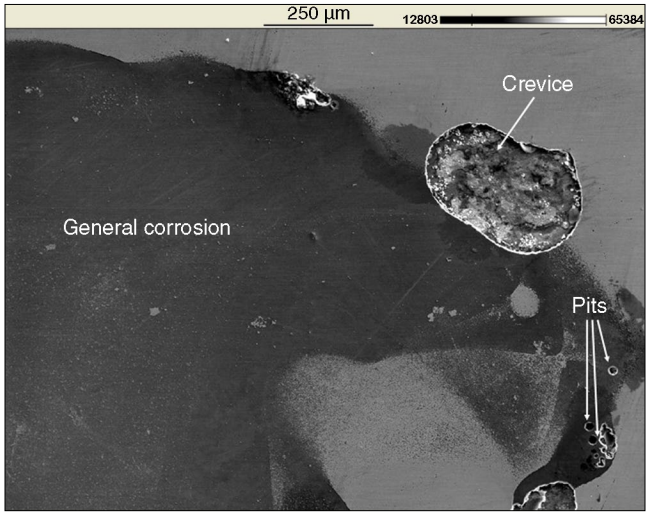

FIGURE 5. *SEM micrograph (scale bar on top) of an Indium-WB-coating after free corrosion test in artificial sweat showing crevice, pits, and generalized corrosion features.*

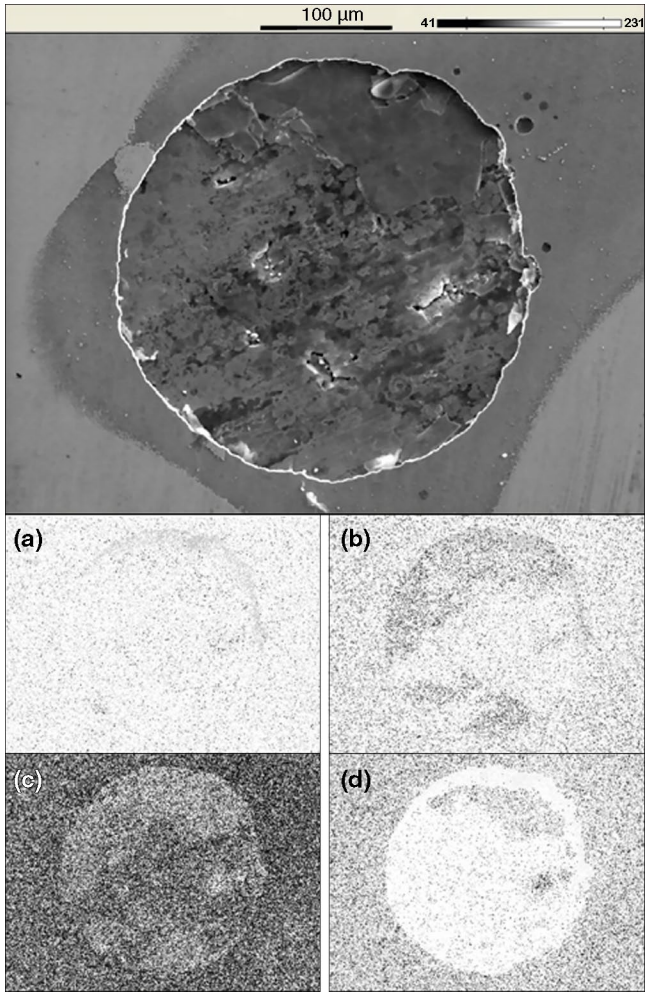

FIGURE 6. *SEM-EDX mapping (scale bar on top) of a crevice corrosion feature; (top) SEM image and the corresponding EDX mapping of (a) chlorine, (b) zinc, (c) copper, (d) and tin.*

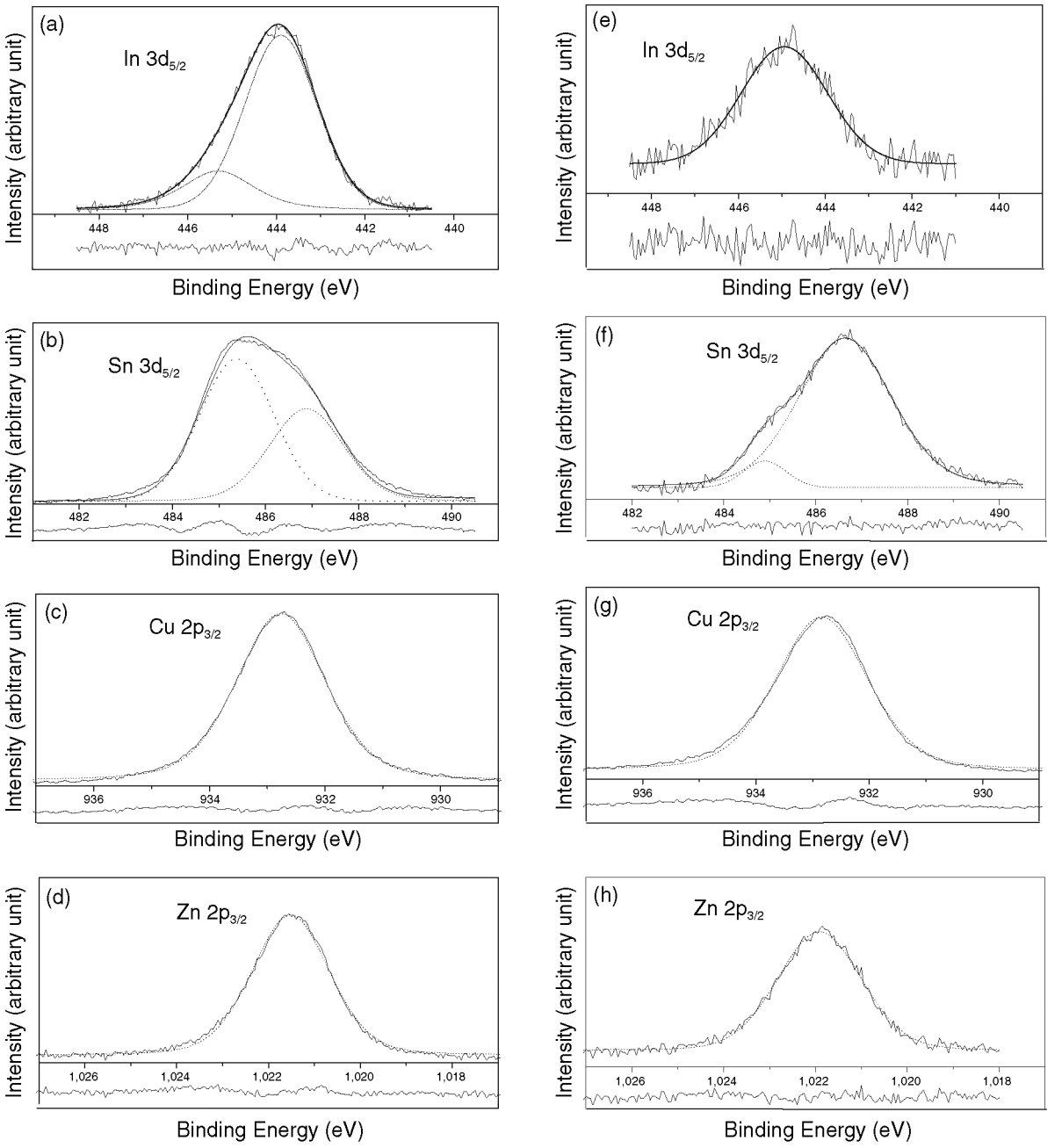

FIGURE 7. *XPS core transaction peaks for indium, tin, copper, and zinc before (a through d) and after (e through h) exposure to artificial sweat solution.*

in view of determining trends in the evolution of the surface composition. Results show that, with respect to the bulk composition, the surface of the Indium-WB-coated samples is enriched in tin and zinc and depleted in copper (Figure 8). It is also worth pointing out that indium and tin are present at the surface in both metallic and oxidized forms, as proven by the binding energy values of the peaks obtained from the deconvolution of their relative XPS peaks (Figures 7[a] and [b]). On the contrary, copper and zinc are present mainly in metallic form as determined by Auger spectra (not shown here). After 24 h exposure to artificial sweat, the peaks related to indium and tin decreased sharply, whereas the copper-related ones were enhanced (Figures 8 and 9).

Oxygen and carbon were also detected at the sample's surface before and after the exposure to the artificial sweat solution. However, it is worth noting that their relative contents display opposite trends; oxygen decreases during the test while carbon increases (Figure 9). Two phenomena can be claimed to justify reasonably this observation:

—dissolution of the oxides that can be removed from the surface

—deposition of insoluble organic and inorganic copper salts

In accordance with the electrochemical results previously discussed, it also seems reasonable that both the phenomena take place at the surface.

On the whole, the data here show that exposure to the sweat solution depletes the surface of indium and tin. That is probably caused by the synergic effect of the acidic environment and of complexing anions, such as acetate and lactate. Once the oxide's top layer is removed, corrosion phenomena involve the layer beneath determining the formation of insoluble copper by-products, which can reasonably account for the dark haloes (Figure 4) displayed by the corroded samples. Eventually, the evolution of the corrosion phenomena leads to the formation of large pits and the complete breakdown of the Indium-WB coating.

CONCLUSIONS

❖ Both electrochemical and free corrosion measurements show that Indium-WB (copper-zinc-tin-indium alloy), a virtually "nickel-free" alloy, in which mechanical and aesthetic characteristics are similar to the electroplated nickel, presents lower anticorrosion properties with respect to the nickel when put in contact with artificial sweat solution. The corrosion mechanism involves the weakening and the partial removal of the indium-tin oxides layer that spontaneously forms at the alloy surface. The removal of this layer allows the starting of pitting corrosion that eventually leads to the coating failure. Therefore, the key point to improve the corrosion performances of Indium-WB is to increase the stability of this oxide layer.

ACKNOWLEDGMENTS

The authors thank D. Petracchi for valuable experimental work. I. Del Pace and Pallotti of Valmet s.r.l. are thanked for supplying the samples in the study as well as very useful discussions.

REFERENCES

1. J.P. Thyssen, H.I. Maibach, *J. Am. Acad. Dermatol.* 58 (2008): p. 1000.
2. A. Pönkä, A. Ekman, *Sci. Total Environ.* 224 (1998): p. 161.
3. D.A. Basketter, G. Briatico-Vangosa, W. Kaestner, C. Lally, W. Bontinck, *Contact Dermatitis* 28 (1993): p. 15.
4. J.P. Thyssen, J.D. Johansen, B.C. Carlsen, T. Menné, *J. Am. Acad. Dermatol.* 61 (2009): p. 799.
5. N.H. Nielsen, T. Menné, *Acta Derm. Venereol.* 72 (1992): p. 456.
6. C. Liden, M. Bruze, T. Menné, *Textbook of Contact Dermatitis*, 2nd ed., eds. R.J.G. Rycroft, T. Menné, P.J. Frosch, J.P. Lepoittevin (Heildelberg, Germany: Springer-Verlag, 2001).
7. B. Meding, C. Liden, N. Berglind, *Contact Dermatitis* 45 (2001): p. 341.
8. R.L. Rietschel, J.F. Fowler, E.M. Warshaw, D. Belsito, V.A. DeLeo, H.I. Maibach, *Dermatitis* 19 (2008): p. 9.
9. J.G. Marks, Jr., D.V. Belsito, V.A. DeLeo, J.F. Fowler, Jr., A.F. Fransway, H.I. Maibach, C.G. Toby Mathias, J.R. Nethercott, R.L. Rietschel, L.E. Rosenthal, E.F. Sherertz, F.J. Storrs, J.S. Taylor, *Am. J. Cont. Dermat.* 6 (1995): p. 160.

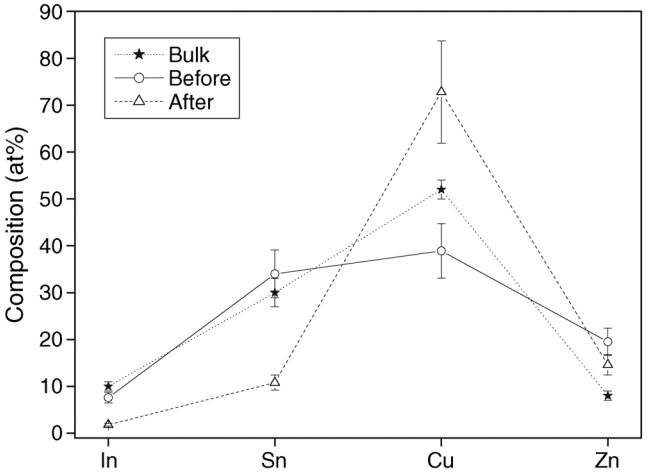

FIGURE 8. *Elemental surface composition relative to the elements constituting the white bronze alloy as determined by XPS before and after the exposure to artificial sweat, compared with the alloy bulk composition.*

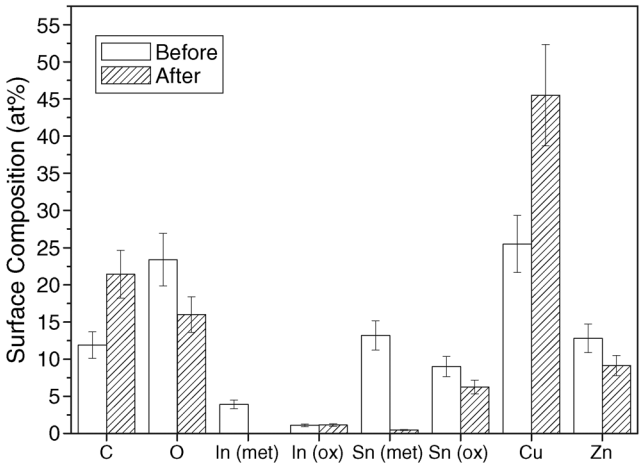

FIGURE 9. *Bar histogram of the semi-quantitative chemical composition of the Indium-WB coatings' surface as determined by XPS before and after the exposure to artificial sweat solution.*

10. N.B. Silveberg, J. Licht, S. Friedler, S. Sethi, T.A. Laude, *Pediat. Dermatol.* 19 (2002): 110.
11. S.E. Jacob, J.N. Moennich, B.A. McKean, M.J. Zirwas, J.S. Taylor, *J. Am. Acad. Dermatol.* 60 (2009): p. 1067.
12. Commission directive 2004/96/EC of 27 September 2004.
13. Commission directive 2008/58/CE of 15 September 2008 and the related technical progress adjustments (30° and 31° Atp).
14. M. Maitz, N. Shevchenko, *J. Biomed. Mater. Res. A* 76 (2006): p. 356.
15. C. Trepanier, M. Tabrizian, L. Yahia, L. Bilodeau, D. Piron, *J. Biomed. Mater. Res.* 43 (1998): p. 433.
16. D.R. Holmes, Jr., A. Lansky, R. Kuntz, M.R. Bell, M. Buchbinder, R. Fortuna, C.D. O'Shaughnessy, J. Popma, *Am. J. Cardiol.* 86 (2000): p. 1073.
17. B. O'Brien, W. Carroll, M. Kelly, *Biomaterials* 23 (2002): p. 1739.
18. M. Mazumder, S. De, S. Trigwell, N. Ali, J. Mehta, *J. Biomater. Sci. Polym.* 14 (2003): p. 1351.
19. U. Kamachi Mudali, P. Shankar, S. Ningshen, R.K. Dayal, H.S. Khatak, B. Raj, *Corros. Sci.* 44 (2002): p. 2183.
20. G. Herting, I. Odnevall Wallinder, C. Leygraf, *J. Food Eng.* 87 (2008): p. 291.
21. C. Liden, E. Rondell, L. Skare, A. Nalbanti, *Contact Dermatitis* 39 (1998): p. 127.

22. F.O. Nestle, H. Speidel, M.O. Speidel, *Nature* 419 (2002): p. 132.
23. I. Rezić, M. Zeiner, I. Steffan, *Monatsh. Chem.* 140 (2009): p. 147.
24. I. Rezić, L. Ćurković, M. Ujević, *Corros. Sci.* 51 (2009): p. 1985.
25. G. Herting, I. Odnevall Wallinder, C. Leygraf, *Corros. Sci.* 49 (2007): p. 103.
26. I. Milošev, T. Kosec, *App. Surf. Sci.* 254 (2007): p. 644.
27. Y. Okazaki, E. Gotoh, *Biomaterials* 26 (2005): p. 11.
28. P. Haudrechy, B. Mantout, A. Frappaz, D. Rousseau, U. Chabeau, M. Faure, A. Claudy, *Contact Dermatitis* 37 (1997): p. 113.
29. I. Milošev, T. Kosec, *Electrochim. Acta* 52 (2007): p. 6799.
30. A. Chiba, S. Sakakura, K. Kobayashi, *J. Mater. Sci.* 32 (1997): p. 1995.
31. G. Moretti, F. Guidi, G. Capobianco, R. Tonini, *J. Mater. Chem.* 11 (2001): p. 922.
32. U. Beck, G. Reiners, I. Urban, H.A. Jehn, U. Kopacz, H. Schack, *Surf. Coat. Technol.* 61 (1993): p. 215.
33. L. Barchi, U. Bardi, S. Caporali, M. Fantini, Al. Scrivani, An. Scrivani, *Prog. Org. Coat.* 67 (2010): p. 146.
34. DIN 50018, "Testing in a Saturated Atmosphere in the Presence of Sulfur Dioxide" (Berlin, Germany: Deutsches Institut Fur Normung E.V. [German National Standard], 1997).
35. A. Survila, Z. Mockus, S. Kanapeckaite, V. Jasulaitiené, R. Juškénas, *Electrochim. Acta* 52 (2007): p. 3067.
36. E.W. Brooman, *Met. Finish.* 99 (2001): p. 100.
37. P. Lalanne, "Electrolyte Composition and Method for the Deposition of Quaternary Copper Alloys," EP patent no. 1930478, 2008.
38. S. Caporali, *Rec. Pat. Corros. Sci.* 1 (2011): p. 8-14.
39. ISO 3160-2:2003, "Watch-Cases and Accessories: Gold Alloy Coverings—Part 2: Determination of Fineness, Thickness, Corrosion Resistance, and Adhesion (Geneva, Switzerland: International Organization for Standardization [ISO], 2003).
40. J.F. Moulder, W.F. Stickle, P.E. Sobol, K.D. Bomben, *Handbook of X-Ray Photoelectron Spectroscopy*, ed. J. Chastain (Waltham, MA: Perkin-Elmer Corporation, 1992).
41. Y.S. Huang, X.T. Zeng, X.F. Hu, F.M. Liu, *Electrochim. Acta* 49 (2004): p. 4313.
42. J.-Y. Fei, G.D. Wilcox, *Surf. Coat. Technol.* 200 (2006): p. 3533.
43. F. Sun, G. Meng, T. Zhang, Y. Shao, F. Wang, C. Dong, X. Li, *Electrochim. Acta* 54 (2009): p. 1578.
44. G. Moretti, F. Guidi, *Corros. Sci.* 44 (2002): p. 2001.
45. G. Kear, B.D. Barker, K.R. Stokes, F.C. Walsh, *Corrosion* 65, 2 (2009): p. 96-104.
46. M. Braun, K. Nobe, *J. Electrochem. Soc.* 126 (1979): p. 1666.
47. E.M. Sheriff, S.-M. Park, *Electrochim. Acta* 51 (2006): p. 4665.
48. M. Itagki, M. Tagaki, K. Wantanabe, *Corros. Sci.* 38 (1996): p. 601.
49. N. Perez, *Electrochemistry and Corrosion Science* (Norwell, MA: Kluwer, 2004).
50. J.F. Watts, J. Wolstenholme, *An Introduction to Surface Analysis by XPS and AES* (Chichester, U.K.: Wiley, 2003).